Heliyon 6 (2020) e03094

Contents lists available at ScienceDirect

Heliyon

journal homepage: www.cell.com/heliyon

Research article

Dependence of electric power flow on solar radiation power in compact photovoltaic system containing SiC-based inverter with spherical Si solar cells

Yuji Ando [a], Takeo Oku [a,*], Masashi Yasuda [b], Kazufumi Ushijima [c], Hiroshi Matsuo [d], Mikio Murozono [e]

[a] Department of Materials Science, The University of Shiga Prefecture, 2500 Hassaka, Hikone, Shiga, 522-8533, Japan
[b] Collaborative Research Center, The University of Shiga Prefecture, 2500 Hassaka, Hikone, Shiga, 522-8533, Japan
[c] U. Design, 2-22 Takatsuka, Hirakata, Osaka, 573-0035, Japan
[d] Micro Vehicle Lab., Ltd., 3-3-2 Tosabori, Nishi-ku, Osaka, 550-0001, Japan
[e] Clean Venture 21 Co., 38 Ishihara Douno-Ushirocho, Kissyouin, Minami-ku, Kyoto, 601-8355, Japan

ARTICLE INFO

Keywords:
Electrical engineering
Energy
Power converter
Energy storage technology
Renewable energy resources
Solar energy
Photovoltaics
Energy sustainability
Materials physics
Solar cell
Maximum power point tracking charge controller
Lithium-ion battery
Direct current-alternating current converter
Silicon carbide
Spherical silicon
Field effect transistor
Schottky diode
Inverter

ABSTRACT

A photovoltaic power generation system suitable for mobile applications was developed. A SiC integrated converter with the maximum power point tracking circuit provided the smallest photovoltaic inverter in ~200 W level. The SiC-based inverter exhibited a peak direct current (DC)-alternating current (AC) conversion efficiency higher than that of conventional Si inverters. A Li-ion laminated battery was mounted in the same housing as the inverter. The weight of entire system containing spherical Si solar cell panels was well below 6 kg. Continuous operation measurements of this system were carried out using four solar cell modules connected in parallel under irradiation by natural sunlight. The total inverter efficiencies under realistic operation conditions were slightly decreased compared with the DC-AC converter values because of loss by the maximum power point tracking device. Even under unstable weather conditions, the system provided power stability without ripples. The behaviors of the output powers of the solar cell, storage battery, and inverter modules were analyzed as a function of the solar radiation power density. The substantial efficiencies of the solar cell modules were dependent on the weather conditions and were approximately 10% on cloudy days. The present compact photovoltaic power generation system with SiC device and spherical Si solar cells is viable for sub kW-class inverter.

1. Introduction

1.1. Advantages of wide bandgap semiconductor materials

Current power device should meet the conditions such as a low ON-resistance, high blocking voltage, and high switching frequency, even at high temperatures. Wide gap semiconductors such as SiC and GaN have been examined as the power devices [1, 2, 3], and they have high voltage endurance, and a thin epitaxial layer is enough to intercept the voltage. Therefore, SiC and GaN switching devices provide lower ON-resistances than the Si devices. Efficiencies of inverters can be improved by a low ON-resistance, and the module size can be reduced by the low ON-resistance and the increased power density. The GaN and SiC devices can be operated at high temperatures, which is due to their good thermal stabilities.

1.2. Reports on photovoltaic inverter with SiC device

After the reports on photovoltaic (PV) inverter equipped with SiC diodes [4] and SiC transistors [5], many works have been reported for the

* Corresponding author.
E-mail address: oku@mat.usp.ac.jp (T. Oku).

https://doi.org/10.1016/j.heliyon.2019.e03094
Received 22 May 2019; Received in revised form 7 November 2019; Accepted 18 December 2019

SiC power converters [6, 7, 8]. Interleaved direct current (DC)-DC converters built with SiC bipolar junction transistors (BJTs) and Schottky barrier diodes (SBDs) were reported [9, 10]. DC-alternating current (AC) converters using SiC metal-oxide-semiconductor field-effect transistors (MOSFETs) and junction field effect transistors (JFETs) were reported [11, 12]. 3 phase inverters equipped with SiC MOSFETs and JFETs were also developed[13, 14]. Furthermore, inverters using all SiC devices were reported [15, 16]. Some authors have reported comparative studies on inverters with SiC and Si devices [17, 18, 19], and SiC converters with photovoltaic system were also reviewed [20]. These SiC devices have been used as switching devices like MOSFETs, JFETs, and BJTs. The commercially obtainable SiC MOSFET is a normally-off device controlled by voltage, which is easy to use. Although the SiC JFET and SiC BJT are not so advanced devices, these devices are expected to provide a reduced resistivity for switching-on, because they have good carrier transport comparing with SiC MOSFET. Properties of normally-off SiC BJT depends on the current, and need a specific circuit. SiC JFET has a *pn* junction with a gate voltage of ~3 V corresponding to the bandgap. The JFET needs a high voltage for switching the gate, and needs a specific circuit. Most of reported works on SiC-based inverters are concerned with applications in multi-kW level.

Benefits of the low ON-resistance for the SiC device have generally been considered to be reduced in sub-kW level inverters. Thus, it is necessary to investigate the effectiveness of SiC devices in sub-kW applications. SiC-equipped inverters in sub kW level were recently reported [21, 22, 23, 24, 25], and have been found to be effective and compact inverters [26, 27, 28, 29]. Such small inverters are useful for various compact and transportable devices.

1.3. Aim of this work

The purpose of the present work was to develop a compact, lightweight SiC-based inverter equipped with a maximum power point tracking (MPPT) circuit and a lithium ion laminated battery. A previously reported SiC inverter with a MPPT system [26, 27, 28, 29] was refined in the present study, and a 15-V Li-ion laminated battery was developed. Based on these technologies, a compact photovoltaic PV power system was constructed using spherical Si modules. The spherical Si solar cell panel is flexible and lightweight, and are appropriate for mobile use [30]. This study also aimed to study the influence of the solar radiation power on the electrical power flow of this PV power generation system. For this purpose, constant measurements of the present system were carried out under the natural sunlight irradiation. The behavior of the output powers of the solar cell, storage battery, and inverter modules were analyzed as a function of the solar radiation power density. The substantial efficiencies of the solar cell and inverter modules under realistic operation conditions were estimated.

2. Experimental

Figure 1(a) shows a schematic of the present photovoltaic power generation system. An MPPT charge controller, Li-ion laminated battery, and DC-AC SiC converter were contained in a single battery-converter unit. Figure 1(b) shows a digital photographic image of the developed battery-converter system. This unit consisted of a photovoltaic converter module and a lithium ion laminated battery module. The PV inverter module contained the MPPT circuit and the DC-AC SiC converter circuit. The MPPT charge controller maximized the photovoltaic output power by controlling load of the panels, and controlled the power supply to the DC-AC part by discharging and charging the lithium ion battery [31]. The DC-AC converter was constructed from a front DC-DC stage with a next DC-AC stage. The DC-DC circuit was constructed from 4 SiC Schottky barrier diodes (STPSC10TH13TI, STMicroelectronics, Tokyo, Japan) [32]. A single-phase full-bridge DC-AC converter consisted of 4 SiC metal-oxide-semiconductor field-effect transistors (SCT3060AL, ROHM Semiconductor, Kyoto, Japan) [33]. The switching frequencies of the pulse width modulation were 200 kHz for the DC-DC parts and 100 kHz for the DC-AC parts. These high switching frequencies made it possible to decrease the size of the PV inverter module. The output power of the present inverter was 150 W. Compared with the reported inverter

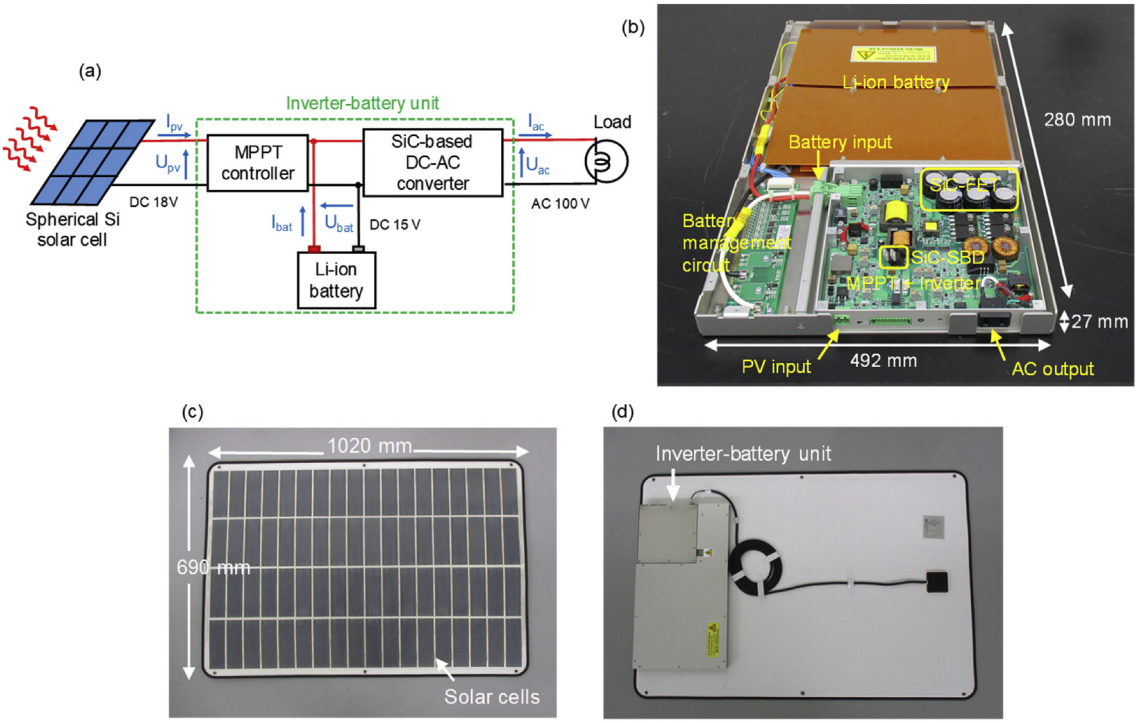

Figure 1. (a) Schematic of the present photovoltaic inverter system. Digital photographs of the (b) inverter-battery unit, (c) top and (d) bottom of the present system.

module [26, 27], the volume and weight of the module were reduced more than ~35%. Optimization of the circuit structure and density provided the present, most compact inverter among ~200 level PV inverter systems [34].

Figures 1(c) and 1(d) show digital photographic images of the present inverter system. A battery-converter unit was attached to the bottom of the solar cell module. The maximum power point voltage and current for the spherical Si panels (CVFM-0540T2-WH, Clean Venture 21, Kyoto, Japan) were 16.2 V and 3.34 A, respectively. The rated output power for one solar cell module was 54 W. The photo-generated voltage was ~14 V, and the output power depended on the solar radiation power.

A $LiMn_2O_4$-based laminated battery module was also developed. This battery consisted of four 3.8 V cells connected in series. To adjust the specifications of the Li-ion battery to those of the spherical Si solar cell module, the rated voltage of the battery was set to 15.2 V and the current capacity was 12 Ah. The thinness of these cells (<10 mm) realized a thin-type power conversion apparatus in which the PV inverter module and battery module were mounted in the same housing. Sizes and weights of modules and the total system are summarized as Table 1. The weight of the total system with a single PV module was well below 5.7 kg.

The output power setting was 150 W, and parallel-connected spherical Si panels were set as the power source. Voltages and currents of the inverter, PV panels, and lithium ion battery were measured simultaneously by power meters (Hioki, PW3336, Nagano, Japan). Interval of the measurement was set as 200 ms, and the data were averaged for every minute. The solar radiation power (Uizin, UIZ-PCM01-LR, Tokyo, Japan), temperature, and humidity (Hioki, LR5001) were measured synchronously. Filament lamps were applied as the load. Conversion efficiencies of individual inverters were estimated by output/input powers.

3. Results and discussion

3.1. Conversion efficiency of the PV inverter

The conversion efficiency of each circuit of the present inverter was characterized independently. The efficiencies of the MPPT circuit (η_{MPPT}) were measured by supplying alternative power to the cell part with the inactive DC-AC converter. In Figure 2(a), the square symbols show η_{MPPT} with respect to DC output power in this 15-V battery measurement. When the DC power was above 23 W, the efficiencies surpassed 92%, and the highest efficiency extended to 96%.Efficiencies of the DC-AC circuit ($\eta_{DC\text{-}AC}$) was investigated for the inactive spherical Si panels. In Figure 2(b), the square symbols show $\eta_{DC\text{-}AC}$ regarding the AC output in this measurement. The efficiency surpassed 82% above 75 W, and the highest efficiency extended to 87%. This peak efficiency was more than 3% higher than that of ordinary inverters [26, 28]. In general, high switching frequencies greatly affect the efficiencies of DC-AC circuit because of the increased switching losses. The superior efficiency of this inverter was therefore attributed to decreased switching losses in the SiC device compared to in Si devices.

To study the influence of the developed 15-V Li-ion battery, similar measurements were carried out using a conventional 12-V $LiFePO_4$-based battery module (O'Cell, IFM12-200E2, Shenzhen, Guangdong, China). In Figures. 2(a) and (b), the circle symbols show the results of the 12-V battery. The difference in efficiencies between the 15-V battery and 12-V battery measurements were below 2% for η_{MPPT} and below 3% for $\eta_{DC\text{-}AC}$. These results indicated that the efficiencies of the DC-AC converter and MPPT circuit were mildly dependent on the battery voltage.

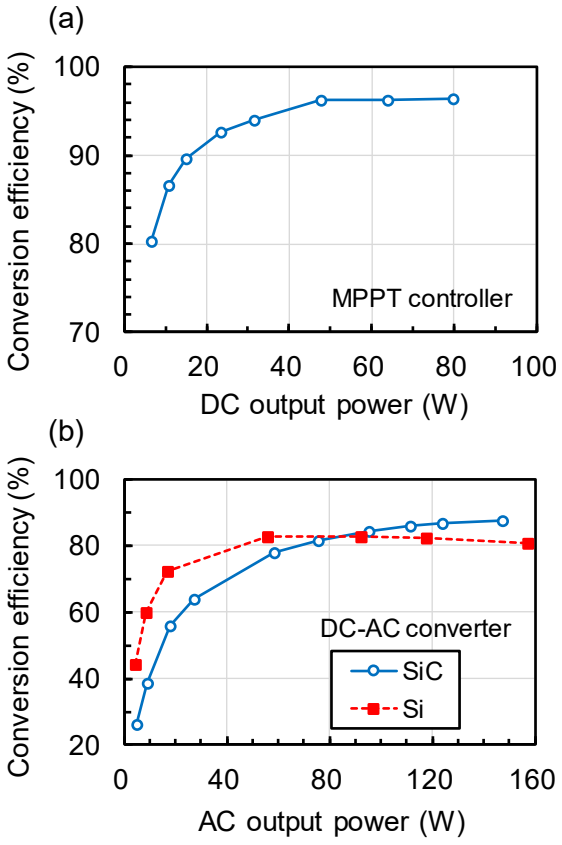

Figure 2. Output power and efficiencies for the (a) MPPT and (b) DC-AC circuits.

3.2. Power loss analysis

Power loss analysis was carried out for the Si- and SiC-based converters according to a previously reported method [28]. Table 2 summarizes the electrical characteristics (ON-resistance (R_{ds}), turn-on loss (E_{on}), and turn-off loss (E_{off}) of the field effect transistor (FET), and forward voltage (V_f) and recovery time (t_{rr}) of the body diode (BD)) assumed for Si and SiC MOSFETs operating at temperature (T) of 25 °C. Reported data for FQPF16N25C (Fairchild semiconductor) and SCT3060AL [31] were used as the parameters. Although the forward current (I_f) across the BD increased the reverse recovery current (I_{rr}), and the I_{rr} of the SiC MOSFET was reduced by short lifetime of minority carriers compared with that of Si MOSFET. It was assumed that $I_{rr} = \alpha I_f$, where $\alpha = 3$ and $\alpha = 1/3$ for Si and SiC, respectively [32].

Comparison between measured and simulated efficiencies for the output AC power. In this calculation, the AC output voltage was set to 100 V and the switching frequencies of the pulse width modulation signal were set to 100 kHz and 20 kHz for the SiC and Si inverters, respectively.

Table 1. Sizes and weights of modules and the total system.

Module	Size (mm^3)	Weight (kg)
Inverter	180 × 175 × 25	0.79
Storage battery	492 × 280 × 27	2.77
Solar cell	1020 × 690 × 5	2.13
Total system (1 PV module)	—	5.69

Table 2. Properties of Si and SiC MOSFETs of the present and commercially available inverters.

Property	Symbol	Unit	SiC	Si	Remarks
FET ON-resistance	R_{ds}	Ω	0.06	0.22	Almost independent of I
FET turn-on loss	E_{on}	μJ	70	180	Measured at $V_t = 300$ V, $I_t = 10$ A
FET turn-off loss	E_{off}	μJ	10	120	Measured at $V_t = 300$ V, $I_t = 10$ A

Satisfactory agreement was obtained between the measured and simulated efficiencies for both inverters. Open circle symbols in Figure 3 show the DC-AC conversion efficiencies regarding the AC output. The DC-AC efficiency for the SiC device surpassed 80% above 75 W. A Si-based commercial inverter (SXCD-300, Daiji Industry, Osaka, Japan) was similarly investigated for the same system. When the output power was larger than 90 W, the present SiC inverter showed superior efficiency to the Si inverter, and this improvement in efficiency reached 7% at an output power of 150 W. For the lower output power than 90 W, the Si inverter showed superior efficiency to the SiC inverter. Loss analysis was carried out to account for this behavior in the DC-AC conversion efficiency.

Contributions of power loss components to the total loss occurring at output powers of 20 W, 75 W, and 150 W are shown in Figures 4(a), 4(b), and 4(c), respectively. In these figures, the total power loss is divided into three components: DC-DC loss ($P_{dc\text{-}dc}$), DC-AC loss ($P_{dc\text{-}ac}$), and non-load loss (P_{nl}) that was independent of the load value. When the power increased, the contributions of the DC-DC and DC-AC losses increased. In contrast, the contribution of the non-load loss became more significant when the output power decreased. Therefore, the decreased DC-DC and DC-AC losses in the SiC inverter were responsible for its superior efficiencies at high power, and the increased non-load loss was responsible for the inferior efficiencies at low power. The non-load loss mainly originated from the filter and transformers equipped in the DC-DC circuit. The decreased DC-DC loss in the SiC inverter was considered to be due to decreased conduction loss in the SiC SBD because of the lower ON-resistance compared with the Si switching diodes. The DC-AC loss was composed of several components.

Contributions of power loss components to the DC-AC loss for 20 W, 75 W, and 150 W are shown in Figures 5(a), 5(b), and 5(c), respectively. The DC-AC power loss is divided into five elements: conduction loss (P_{fet}), turn-on loss (P_{on}) and turn-off loss (P_{off}) of the FET, and conduction loss (P_{bd}) and reverse recovery loss (P_{rr}) of the body diode. The conduction losses (P_{fet} and P_{bd}) were less important since the most of the DC-AC losses were P_{on}, P_{off} and P_{rr}. The reduced recovery loss in the SiC MOSFET was mainly responsible for the decreased loss in the SiC DC-AC circuit. To reduce the module size, the switching frequency of pulse width modulation was raised from 20 kHz for the Si inverter to 100 kHz for the SiC inverter, which was expected to significantly increase the switching losses for the SiC device. However, the switching losses were not so much in the SiC inverter, which was due to the smaller turn-on and turn-off delay times of the SiC MOSFET.

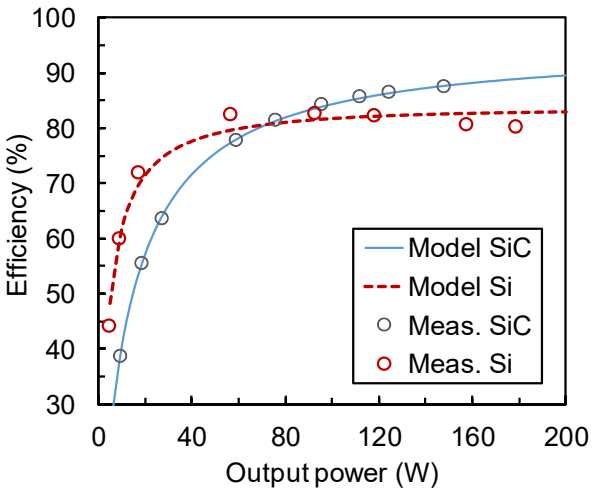

Figure 3. Measured (circles) and simulated (lines) efficiencies of the developed SiC inverter and commercially available Si inverter.

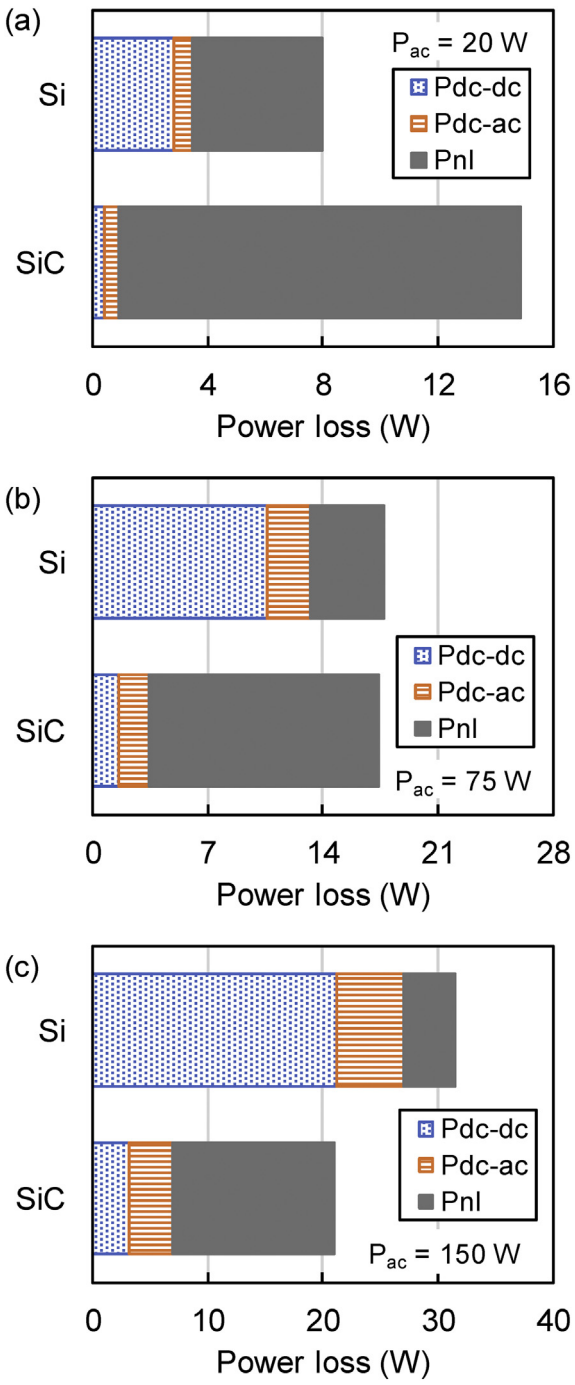

Figure 4. Contributions of DC-DC power loss components to the total loss for (a) 20 W, (b) 75 W, and (c) 150 W.

3.3. *Effect of number of solar cell modules*

To investigate the substantial output power of the PV modules, one to four PV modules were connected in parallel and the resulting system was operated under irradiation by natural sunlight. The load power was fixed at 74 W. The powers at the solar cell (P_{pv}), battery (P_{bat}), and output (P_{ac}) parts of the inverter were measured synchronously. The temperature, humidity, and solar radiation power density (p_{sol}) were also monitored during the measurement.

Figure 6(a) shows the measured P_{pv} as a function of p_{sol} in a typical measurement using a single PV module. An ideal curve expected from the rated output power of 54 W is also shown. The measured output power

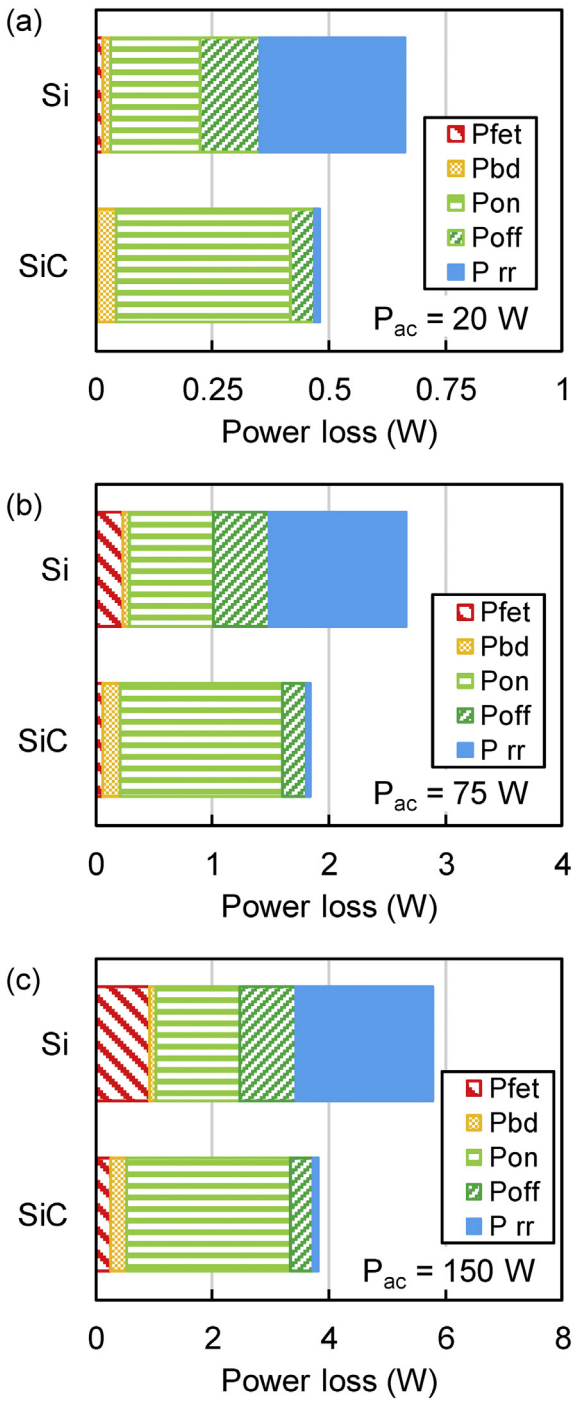

Figure 5. Contributions of power loss components to the DC-AC loss for (a) 20 W, (b) 75 W, and (c) 150 W.

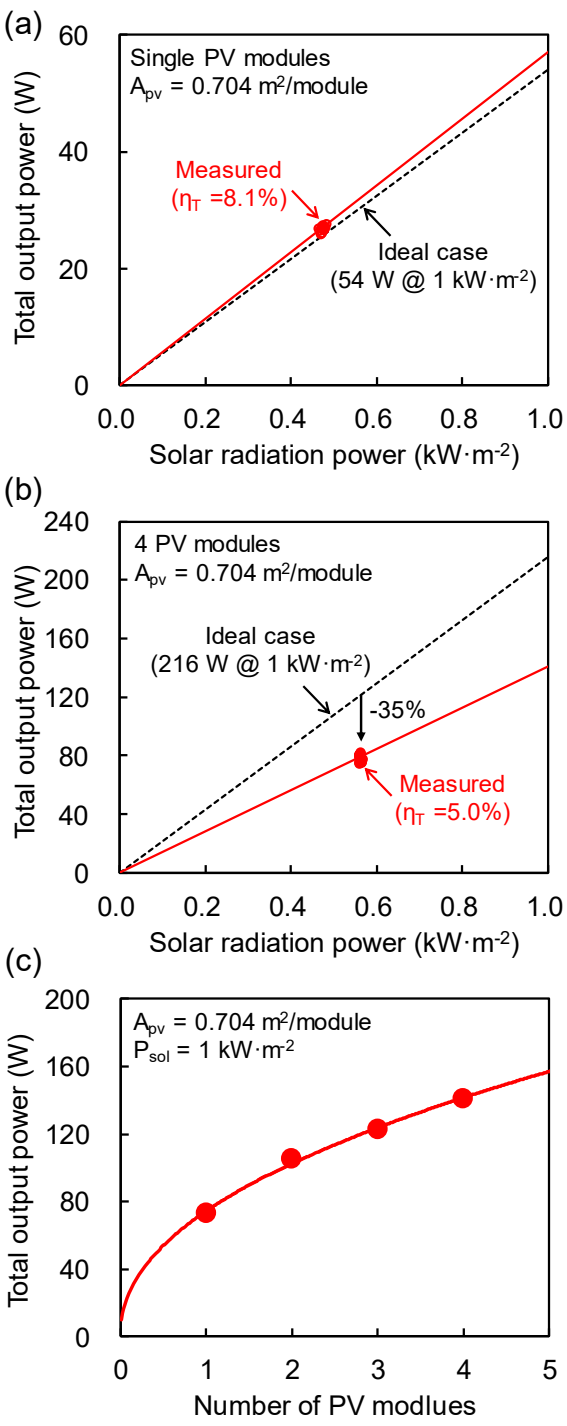

Figure 6. Total output power versus the solar radiation power density for measurements using a (a) single PV module and (b) four PV modules connected in parallel. (c) PV module number dependence of the total output power extrapolated to a solar radiation power density of 1 kW m^{-2}.

was generally located along this ideal curve. Figure 6(b) shows the results using four PV modules connected in parallel. The measured total power was decreased by 35% compared with that expected from the rated output power of 54 W/module. Figure 6(c) shows the PV module number dependence of the total output power extrapolated to a solar radiation power density of 1 kW m^{-2}. The power density per module decreased with increasing number of PV modules. This decrease in output power density was mainly due to the variation in electrical characteristics of individual PV modules. PV modules were connected in parallel in this measurement setup, and small variations in open circuit voltages would significantly lower the total efficiency.

3.4. *Efficiency changes under the natural sunlight*

To study power flow of the photovoltaic power generation system, efficiency changes were measured under the natural sunlight irradiation. First, the measurement was performed under cloudy conditions. Four PV modules were connected in parallel and the load power was set to 20 W. Electric powers P_{pv}, P_{bat}, and P_{ac} are shown in Figure 7(a) η_{MPPT}, $\eta_{DC\text{-}AC}$, and the total inverter efficiency (η_{TOT}) are also shown in Figure 7(b). In the present work, total efficiencies that were originally introduced by

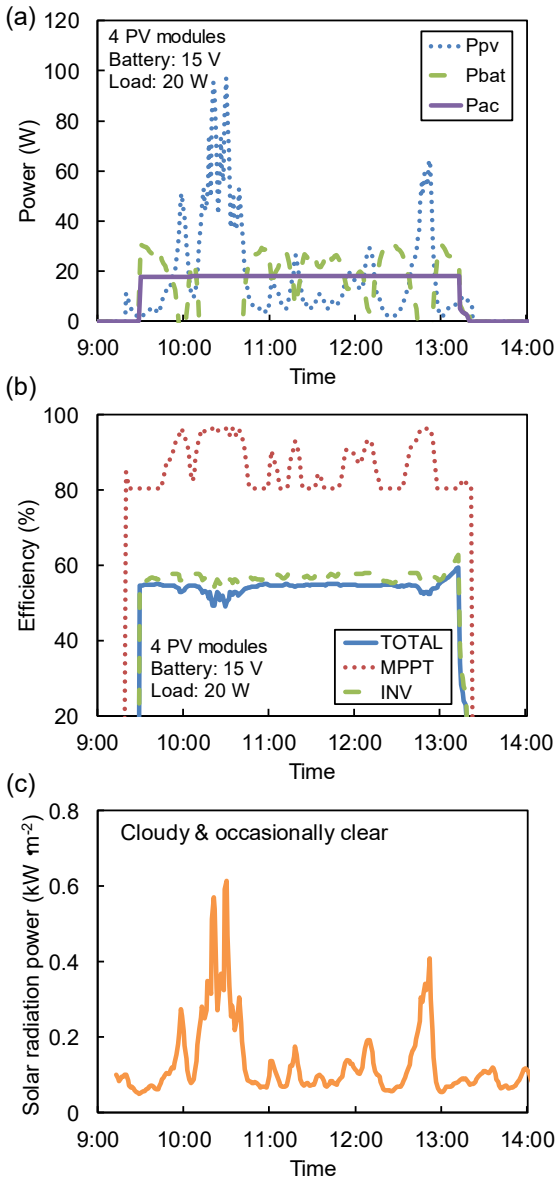

Figure 7. (a) power at the PV (dotted), AC (solid), and battery (broken) parts of the inverter, (b) efficiencies of the MPPT (dotted), DC-AC part (broken), and total system (solid), and (c) solar radiation density. The measurement was carried out using four PV modules at a load power of 20 W. The weather conditions were cloudy and occasionally clear.

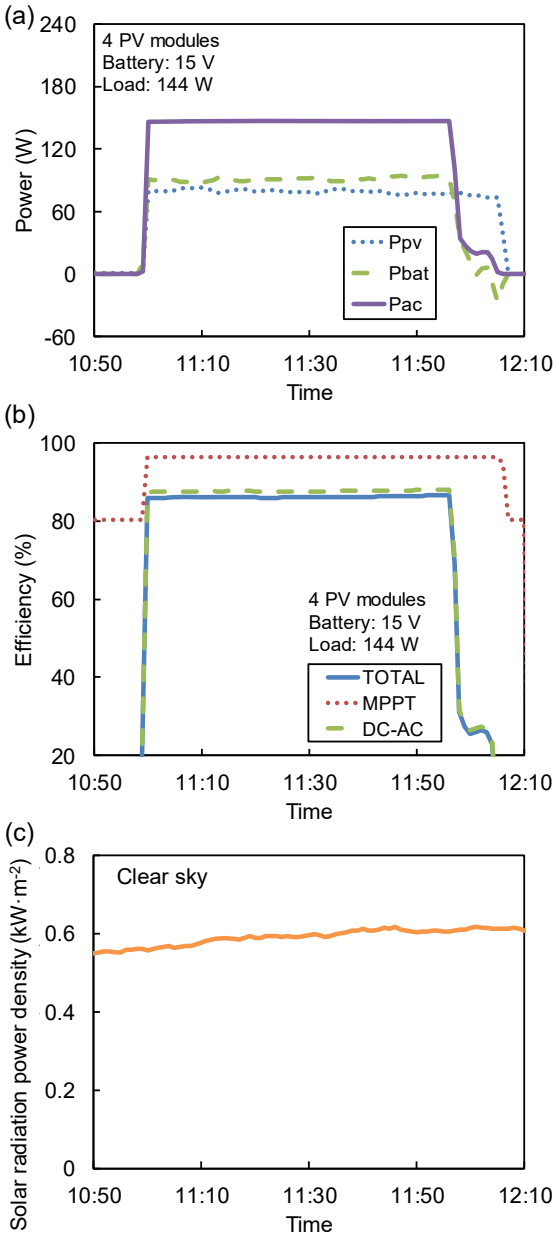

Figure 8. (a) Power at the PV (dotted), AC (solid), and battery (broken) parts of the inverter, (b) efficiencies of the MPPT (dotted), DC-AC part (broken), and total system (solid), and (c) solar radiation density. The measurement was carried out using four PV modules at a load power of 144 W. The weather conditions were clear.

Haeberlin et al. [35] was adjusted to contain the battery, which is given by

$$\eta_{TOT} = \frac{P_{ac}}{P_{pv} + P_{bat}} \tag{1}$$

Because the weather conditions were cloudy and occasionally clear, considerable variation was observed in p_{sol}, as shown in Figure 7(c). Consequently, large instability was seen in P_{pv} and P_{bat}, as shown in Figure 7(a). Even under unstable weather conditions, P_{ac} was very stable and no ripples were observed. The total efficiencies were in the range of 50–60%, which was due tothe low power of 20 W. Under these conditions, the efficiencies were predominantly controlled by the transformers and filter circuit in the DC-DC part [34].

A similar measurement was then performed under clear sky conditions. Four PV modules were connected in parallel at 144 W Figure 8(a), (b), and (c) show the changes in electric powers (P_{pv}, P_{bat}, and P_{ac}), conversion efficiencies (η_{MPPT}, $\eta_{DC\text{-}AC}$, and η_{TOT}), and p_{sol}, respectively. Because the weather conditions were clear, p_{sol} was relatively stable and was around 0.6 kW m^{-2}. Thus, no significant instability was seen for P_{pv} or P_{bat}. The total efficiencies were in the range of 86–87%.

Total efficiencies were also measured under 30 W, 54 W, 74 W, 90 W, 110 W, and 125 W. The total inverter efficiencies defined by Eq. (1) were calculated as time averages from measurements spanning several hours. Figure 9 shows η_{TOT} as a function of P_{ac}. A peak η_{TOT} of 86.1% was obtained at the load power of 144 W. The total efficiencies of the inverter under realistic operation conditions were generally decreased compared with the DC-AC converter values, which is due to the MPPT circuit loss. But, the lowering of efficiencies was only a few percent.

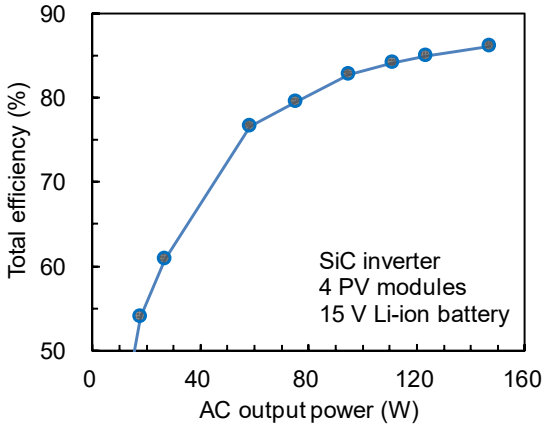

Figure 9. Output power and efficiencies for the inverter under realistic operation conditions.

3.5. Output power and solar radiation density

The relation between the solar radiation power density and the output powers was analyzed from the data of the continuous operation measurements. Figure 10(a), (b), and (c) show P_{pv}, P_{bat}, and P_{ac} as a function of p_{sol}, respectively, which were calculated from the data shown in Figure 4. Because the weather conditions were cloudy and occasionally clear, p_{sol} varied widely. As a result, an almost linear correlation was obtained between P_{pv} and p_{sol}. When p_{sol} was lower than 0.2 kW m^{-2}, P_{bat} was positive which indicated discharging of the battery. Under these conditions, the Li-ion battery supplied the power to compensate for the shortage of P_{pv}. When p_{sol} surpassed 0.2 kW m^{-2}, P_{bat} was negative which indicated charging of the battery. Under these conditions, the electric power supplied by the spherical Si panel was sufficient to supply the system and charge the Li-ion battery. When p_{sol} surpassed 0.5 kW m^{-2}, the slope of P_{pv} tended to decrease. When the battery management circuit sensed an overcharge of the battery, it interrupted the flow of current into the battery, so P_{pv} was suppressed. The operation of the battery management circuit was therefore responsible for this nonlinearity. The dependence of P_{ac} on p_{sol} was very minimal. Figures. 10(a) and (b) also show linear line fit results based on the following equations:

$$P_{pv} = \eta_{pv} A_{pv} (p_{sol} - p_{th}) \tag{2}$$

$$P_{bat} = \frac{P_{ac}}{\eta_{TOT}} - P_{pv} \tag{3}$$

In these expressions, A_{pv} is the active area of the cell panel. The efficiency of the PV modules (η_{pv}) and the threshold power density (p_{th}) were used as fitting parameters. Assuming the active area of the solar cell was 2.16 m^2, η_{pv} was estimated to be 9.7%. The threshold power density was approximately 0.04 kW m^{-2}. Similar measurements were performed on different days. A reasonable correlation was obtained between P_{pv} and p_{sol}, and the intersection point was around 0.04 kW m^{-2}. The physical origin of this threshold is currently unclear, and the input voltage regulation scheme used in the MPPT charge controller may have been responsible for this.

Figure 11(a), (b), and (c) show P_{pv}, P_{bat}, and P_{ac} as a function of p_{sol}, respectively, which were calculated from the data in Figure 5. Because the weather conditions were clear, a clear correlation was not obtained between P_{pv} and p_{sol}. P_{bat} was positive throughout the entire measurement. Under these conditions, the Li-ion battery supplied the power to fill in the shortage of P_{pv}. The dependence of P_{ac} on p_{sol} was very minimal. Figures. 11(a) and (b) also show linear line fit results based on Eqs. (2) and (3). The threshold power density was assumed to be 0.04 kW m^{-2}. Assuming the active area of the solar cell was 2.16 m^2, η_{pv} was estimated

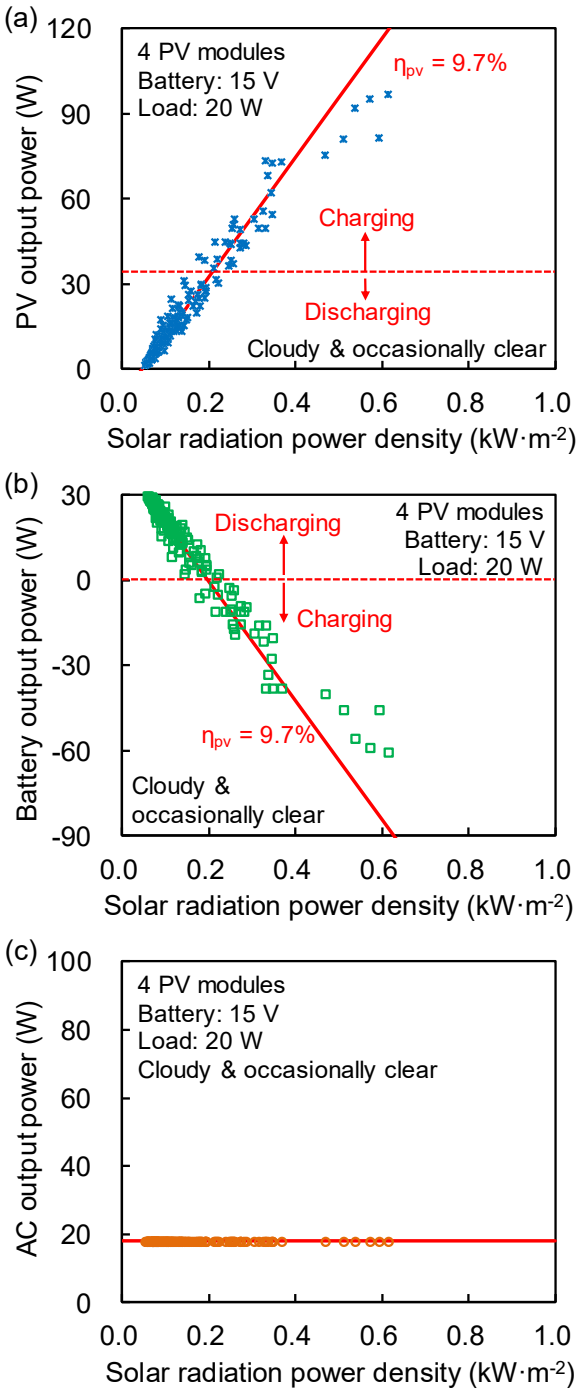

Figure 10. (a) Photovoltaic output, (b) battery output, and (c) AC output powers versus solar radiation density.

to be 6.6%. Similar measurements were performed on different days. Measured η_{pv} values were approximately 6%–7% on clear sky days and approximately 9%–10% on cloudy days. This lower efficiency under clear sky conditions was due to the power loss of the wiring cables and to the heating of the solar cell modules.

3.6. Estimation of battery duration

Measurements on the battery duration (t_{bat}) were performed while the spherical Si panel was not operated. Figure 12 shows the measured and calculated relationships between t_{bat} and P_{ac}. In the calculation, t_{bat} was estimated by

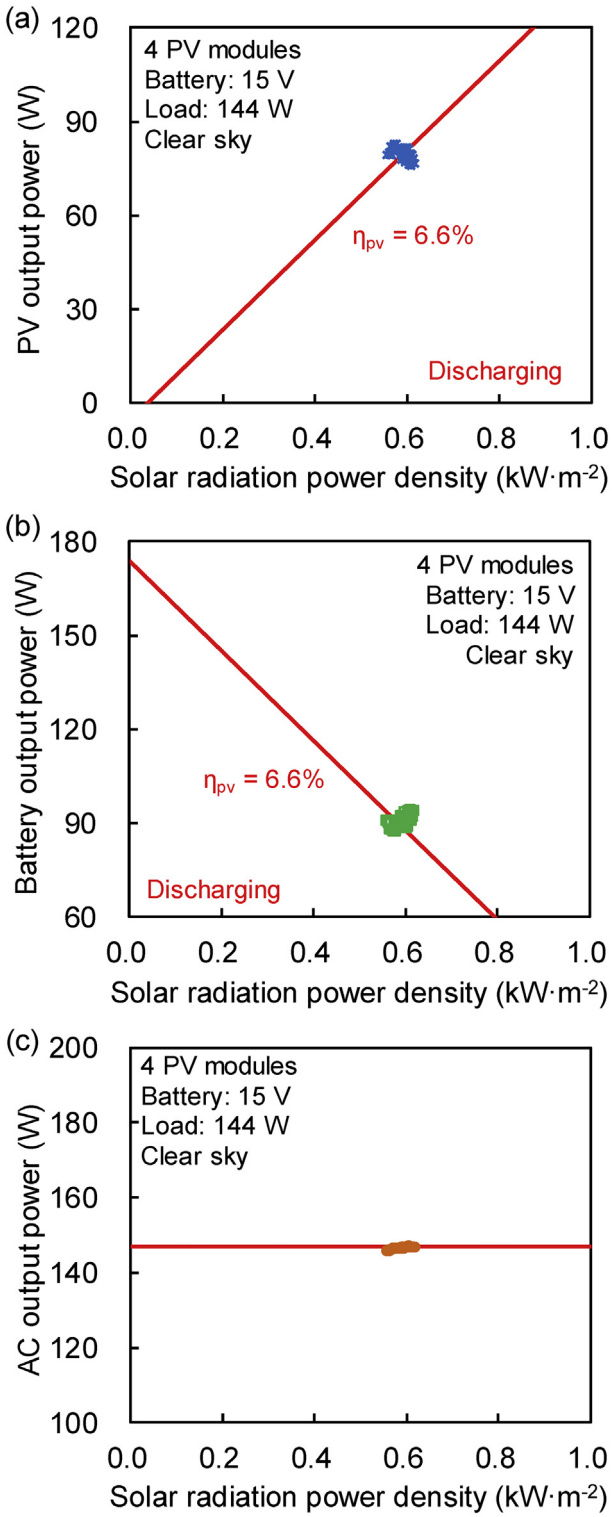

Figure 11. (a) PV output power, (b) battery output power, and (c) AC output power versus the solar radiation density.

$$t_{bat}(P_{ac}, Q_{bat}) = \frac{Q_{bat} V_{bat} \eta_{inv}(P_{ac})}{P_{ac}} \quad (4)$$

V_{bat} is the battery voltage, and Q_{bat} is the battery capacity. η_{inv} (P_{ac}) is the inverter efficiency as a function of P_{ac}. Q_{bat}, V_{bat}, and the series resistance were set to 12 Ah, 15 V, and 1 Ω, respectively. The measured values agreed well with the calculated ones. Figure 12 also shows previously reported data for the SiC system reported previously [28]. The

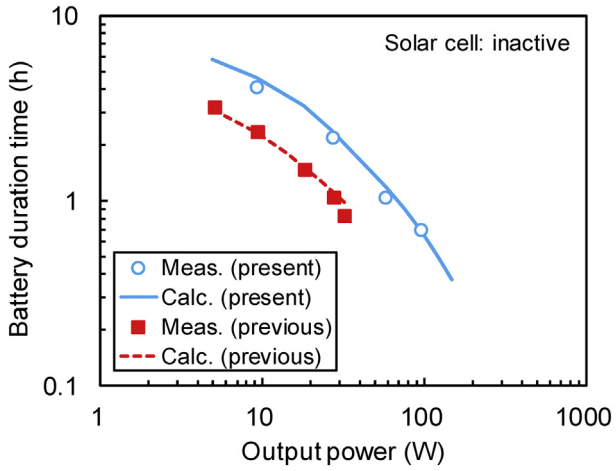

Figure 12. Measured and calculated battery durations versus the AC output power for the developed SiC inverter and commercially available Si inverter. The solar cell was inactive in these calculations and measurements.

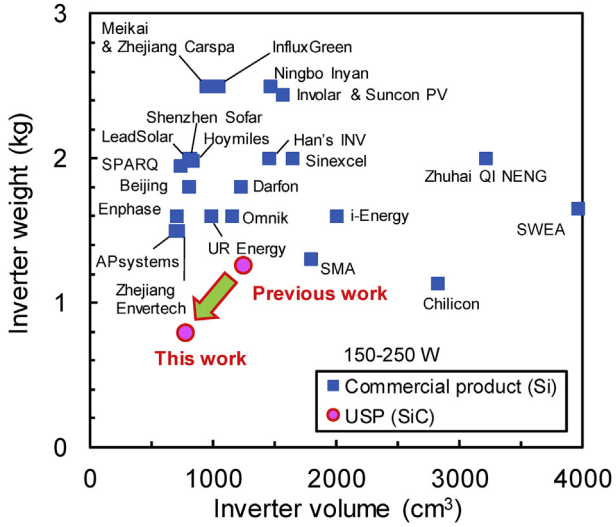

Figure 13. Volumes and weights for the ~200 W class inverters.

developed SiC system exhibited a duration twice as long as that of the reported SiC system.

3.7. Comparison of inverter size

Figure 13 shows the weight of the developed inverter as a function of its volume. Compared with the reported system [26, 27], the volume and weight were reduced by ~40%. Optimization of the circuit design provided the reduced size. Figure 13 also shows the volumes and weights for the ~200 W class inverters, and the developed system was the most compact one [34].

4. Conclusions

A PV power generation system suitable for mobile applications was developed. The MPPT equipped SiC inverter achieved small volume and light weight among ~200 W level photovoltaicinverters. Compared with the previous system, the volume and weight decreased by ~40%. The conversion efficiencies of the DC-AC part and MPPT circuits increased to 87% and 96%, respectively. The SiC-based inverter exhibited a peak efficiency for the DC-AC circuit that was more than 3% higher than that of

the ordinary Si-based inverter. The conversion efficiency of the present SiC inverter was improved by 7% at 150 W. Loss analysis indicated that this improvement was due to decreased conduction loss in the SiC SBD and suppressed the loss by recovery and switchingfor the MOSFET. A Li-ion laminated battery was mounted in the same housing as the inverter. The weight of the total system containing the spherical Si panel was well below 5.7 kg. The measured output powers of four PV modules connected in parallel were decreased by 35% compared to those expected from the rated power of a 54 W/module. Continuous operation measurements of this system were carried out using four PV modules under irradiation by natural sunlight. The total inverter efficiencies under realistic operation conditions were slightly decreased comparing with the DC-AC circuit because of the loss of the MPPT circuit. Even under unstable weather conditions, this system demonstrated a stable output power without ripples. The behaviors of the output powers of the cells, storage battery, and converter modules were analyzed as a function of p_{sol}. The substantial efficiencies of the solar cell modules were dependent on the weather conditions and were approximately 9%–10% on cloudy days. The small volume, light weight, and good efficiency and stability showed the usefulness of the SiC devices and spherical Si solar cells for sub kW level compact photovoltaic inverter. Such systems would be useful for various compact and transportable devices.

Declarations

Author contribution statement

Yuji Ando: Conceived and designed the experiments; Performed the experiments; Analyzed and interpreted the data; Wrote the paper.

Takeo Oku: Conceived and designed the experiments; Analyzed and interpreted the data; Wrote the paper.

Masashi Yasuda & Hiroshi Matsuo: Conceived and designed the experiments; Contributed reagents, materials, analysis tools or data.

Kazufumi Ushijima: Conceived and designed the experiments; Performed the experiments; Contributed reagents, materials, analysis tools or data.

Mikio Murozono: Contributed reagents, materials, analysis tools or data.

Funding statement

This work was supported by the Super Cluster Program of Japan Science and Technology Agency (JST).

Competing interest statement

The authors declare no conflict of interest.

Additional information

No additional information is available for this paper.

References

[1] A.A. Labedev, V.E. Chelnokov, Wide-gap semiconductors for high-power electronics, Semiconductors 33 (1999) 999–1001.
[2] H. Okumura, Present status and future prospect of widegap semiconductor high-power devices, Jpn. J. Appl. Phys. 45 (2006) 7565–7586, 2006.
[3] U.K. Mishra, L. Shen, T.E. Kazior, Y.F. Wu, GaN-based RF power devices and amplifiers, Proc. IEEE 96 (2008) 287–305.
[4] F. Phlippen, B. Burger, A new high voltage Schottky diode based on silicon-carbide (SiC), in: Proceedings of 9th European Conference Power Electronics and Applications, (EPE 2001) (Graz, Austria, 27–28 August 2001), 2001, 00259.
[5] O. Stalter, B. Burger, S. Lehrmann, Silicon carbide (SiC) D-MOS for grid-feeding solar inverters, in: 12th European Conference on Power Electronics and Applications (EPE 2007), (Aalborg, Denmark, 2–5 September 2007), 2007, pp. 1–10.
[6] M. Chinthavali, H. Zhang, L.M. Tolbert, B. Ozpineci, Update on SiC-based inverter technology, in: Electronics Conference (COBEP '09), (Bonito-Mato Grosso Do Sul, Brazil, 27 September–1 October 2009), 2009, pp. 71–79.
[7] A. Yamane, K. Koyanagi, M. Kozako, K. Fuji, M. Hikita, Fabrication and evaluation of SiC inverter using SiC-MOSFET, in: IEEE 10th International Conference on Power Electronics and Drive Systems, (PEDS 2013) (Kitakyushu, Japan, 22–25 April 2013), 2013, pp. 1029–1032.
[8] L. Li, C. Li, Y. Cao, F. Wang, Recent progress of SiC power devices and applications, IEEJ Trans. Electr. Electron. Eng. 8 (2013) 515. C.N.M.521.
[9] A. Hensel, C. Wilhelm, D. Kranzer, Development of a boost converter for PV systems based on SiC BJTs, in: Proc. 2011-14th European Conference on Power Electronics and Applications (EPE 2011), (Birmingham, UK, 30 August–1 September 2011), 2011, pp. 1–7.
[10] C.N.M. Ho, H. Breuninger, S. Pettersson, G. Escobar, A. Coccia, N. Oikonomous, Practical implementation of an interleaved boost converter using SiC diodes for PV applications, in: 8th International Conference on Power Electronics (ICPE 2011-ECCE Asia), (Jeju, Korea, 30 May–3 June 2011), 2011, pp. 372–379.
[11] B. Burger, D. Kranzer, O. Stalter, Cost reduction of PV-inverters with SiC-DMOSFETs, in: 5th International Conference on Integrated Power Systems (CIPS 2008), (Nuremberg, Germany, 11–13 March 2008), 2008, pp. 1–5.
[12] D. Kranzer, C. Wilhelm, F. Reiners, B. Burger, Application of normally-off SiC-JFETs in photovoltaic inverters, in: 13th European Conference on Power Electronics and Applications (EPE 2009), (Barcelona, Spain, 8–10 September 2009), 2009, pp. 1–6.
[13] B. Burger, D. Kranzer, O. Stalter, Efficiency improvement of PV inverters with SiC-DMOSFETs, Mater. Sci. Forum 600–603 (2009) 1231–1234.
[14] O. Stalter, D. Kranzer, S. Rogalla, B. Burger, Advanced solar power electronics, in: Proceedings of 22nd International Symposium on Power Semiconductor Devices & ICs (ISPSD 2010), (Hiroshima, Japan, 6–10 June 2010), 2010, pp. 3–10.
[15] D. De, A. Castellazzi, A. Solomon, A. Trentin, M. Minami, T. Hikihara, An all SiC MOSFET high performance PV converter cell, in: 15th European Conference on Power Electronics and Applications (EPE 2013), (Lille, France, 2–6 September 2013), 2013, pp. 1–10.
[16] N. Nashida, Y. Hinata, M. Horio, R. Yamada, Y. Ikeda, All-SiC power module for photovoltaic power conditioner system, in: IEEE 26th International Symposium on Power Semiconductor Devices & IC's (ISPSD 2014), (Waikoloa, HI, USA, 15–19 June 2014), 2014, pp. 342–345.
[17] R.M. Burkart, J.W. Kolar, Comparative evaluation of SiC and Si PV inverter systems based on power density and efficiency as indicators of initial cost and operating revenue, in: IEEE 14th Workshop on Control and Modeling for Power Electronics (COMPEL), (Salt Lake City, UT, 23-26 June 2013), 2013, pp. 1–6.
[18] C. Sintamarean, F. Blaabjerg, H. Wang, Comprehensive evaluation on efficiency and thermal loading of associated Si and SiC based PV inverter applications, in: IECON 2013 – 39th Annual Conference on IEEE Industrial Electronics Society, (Vienna, Austria, 10-13 November 2013), 2013, pp. 555–560.
[19] C.H.M. Ho, H. Breuninger, S. Pettersson, G. Escobar, F. Canales, A comparative performance study of an interleaved boost converter using commercial Si and SiC diodes for PV Applications, IEEE Trans. Power Electron. 28 (2013) 289–299.
[20] T. Kim, M. Jang, V.G. Agelidis, Current status of silicon carbide power devices and their application in photovoltaic converters, IEEE ECCE Asia DownUnder (ECCE Asia) (2013) 555–559 (Melbourne, Australia, 3-6 June 2013).
[21] T. Oku, T. Matsumoto, K. Hiramatsu, M. Yasuda, A. Shimono, Y. Takeda, M. Murozono, Construction and characterization of spherical Si solar cells combined with SiC electric power inverter, AIP Conference Proceeding 1649 (2015) 79–83.
[22] T. Oku, T. Matsumoto, K. Hiramatsu, M. Yasuda, Y. Ohishi, A. Shimono, Y. Takeda, M. Murozono, Construction and evaluation of photovoltaic power generation and power storage system using SiC field-effect transistor inverter, AIP Conference Proceeding 1709 (2016), 020024–1–10.
[23] T. Matsumoto, T. Oku, K. Hiramatsu, M. Yasuda, Y. Shirahata, A. Shimono, Y. Takeda, M. Murozono, Evaluation of photovoltaic power generation system using spherical silicon solar cells and SiC–FET inverter, AIP Conference Proceeding 1709 (2016), 020023–1–6.
[24] T. Oku, Solar Cells and Energy Materials, De Gruyter, Berlin, Germany, 2017.
[25] Y. Ando, Y. Shirahata, T. Oku, T. Matsumoto, Y. Ohishi, M. Yasuda, A. Shimono, Y. Takeda, M. Murozono, Comparison between SiC- and Si-based inverters for photovoltaic power generation systems, J. Power Energy Eng. 5 (2017) 30–40.
[26] T. Oku, Y. Ando, M. Yasuda, Y. Shirahata, K. Ushijima, M. Murozono, Construction of photovoltaic power generation-storage system using an inverter with SiC FET and SBD, Advances in Energy and Power 5 (2017) 7–12.
[27] Y. Ando, T. Oku, M. Yasuda, Y. Shirahata, K. Ushijima, M. Murozono, A compact SiC photovoltaic inverter with maximum power point tracking function, Sol. Energy 141 (2017) 228–235.
[28] Y. Ando, T. Oku, M. Yasuda, Y. Shirahata, K. Ushijima, M. Murozono, Comparative study of SiC- and Si-based photovoltaic inverters, AIP Conference Proceeding 1807 (2017), 020020–1–9.
[29] Y. Ando, T. Oku, M. Yasuda, K. Ushijima, M. Murozono, Transportable photovoltaic power generation system utilizing a SiC inverter and spherical Si solar cells, Technologies 5 (2017), 18–1–11.
[30] T. Oku, M. Kanayama, Y. Ono, T. Akiyama, Y. Kanamori, M. Murozono, Microstructures, (2014). Optical and photoelectric conversion properties of spherical silicon solar cells with anti-reflection SnO_x:F thin films, Jpn. J. Appl. Phys. 53 (2014), 05FJ03–1–7.
[31] Texas Instruments, Datasheet of BQ24650 – Synchronous Switching-Mode Battery Charge Controller for Solar Power with Maximum Power point Tracking, 2016. Available online, http://www.ti.com/lit/ds/symlink/bq24650.pdf.

[32] STMicroelectronics, Datasheet of STPSC10TH13TI – Dual 650 V Power Schottky Silicon Carbide Diode in Series, 2016. Available online, http://www.st.com/content/ccc/resource/technical/document/datasheet/4d/91/ac/60/b4/d0/44/3e/DM00086244.pdf/files/DM00086244.pdf/jcr:content/translations/en.DM00086244.pdf.

[33] ROHM Semiconductor, Datasheet of SCT3060AL – N-Channel SiC Power MOSFET, 2016. Available online, http://www.rohm.com/web/global/datasheet/SCT3060AL/sct3060al-e.

[34] Y. Ando, T. Oku, M. Yasuda, K. Ushijima, H. Matsuo, M. Murozono, A state-of-the-art compact SiC photovoltaic inverter with maximum power point tracking function, AIP Conference Proceeding 1929 (2018), 020002–1–9.

[35] H. Haeberlin, L. Borgan, M. Kaempfer, U. Zwahlen, Total efficiency ηtot – a new quantity for better characterization of grid-connected PV inverters, in: 20th European Photovoltaic Solar Cell Energy Conference, (Barcelona, Spain, 6–10 June 2005), 2005, pp. 1–4.